Compliance Control of a Cable-Suspended Aerial Manipulator using Hierarchical Control Framework

Chiara Gabellieri[1], Yuri S Sarkisov[2,3], Andre Coelho[2], Lucia Pallottino[1], Konstantin Kondak[2], Min Jun Kim[2]

Abstract— **Aerial robotic manipulation is an emergent trend that poses several challenges. To overcome some of these, the DLR cable-Suspended Aerial Manipulator (SAM) has been envisioned. SAM is composed of a fully actuated multi-rotor anchored to a main carrier through a cable and a KUKA LWR attached below the multi-rotor. This work presents a control method to allow SAM, which is a holonomically constrained system, to perform such interaction tasks using a hierarchical control framework. Within this framework, compliance control of the manipulator end-effector is considered to have the highest priority. The second priority is the control of the oscillations induced by, for example, the motion of the arm or physical contact with the environment. A third priority task is related to the internal motion of the manipulator. The proposed approach is validated through simulations and experiments.**

I. INTRODUCTION

While more classical applications of aerial robots have mainly devoted them to visual exploration of the environment, during the last decade an extensive research effort has been put into aerial physical interaction. Many results have been collected in the field of aerial manipulation, where the main tasks consist of load transportation, wrench exertion, and structural construction [1]. Promising application areas for aerial manipulators are industrial inspection and maintenance [2]. To realize physical interactions, aerial platforms have been equipped with rigid tools [3], cables [4] grippers [5], and manipulators [6].

Among the main challenges are the typical underactuation, coupled dynamics of the multi-rotors, and an unstable base that distinguishes them from the ground counterpart. On the other hand, Unmanned Aerial Vehicles (UAVs) "usually have stringent payload weight constraints and therefore cannot accommodate industrial dexterous robotic manipulators" [1]. Eventually, safety still represents a crucial issue for aerial manipulation [7].

Whereas different works presenting experiments with simple arms characterized by two [8] or three degrees of freedom DoFs [9], [10] can be found in the literature, there are very few examples of experiments with more complex manipulators, especially due to the aforementioned payload limitations. However, a fully actuated robotic arm largely enhances the manipulation capability of the aerial platform,

[1]Centro di Ricerca E. Piaggio and Dipartimento di Ingegneria dell'Informazione, Università di Pisa, Pisa, Italia

[2]Institute of Robotics and Mechatronics, German Aerospace Center (DLR), Wessling, Germany

[3] Space CREI, Skolkovo Institute of Science and Technology (Skoltech), Moscow, Russia
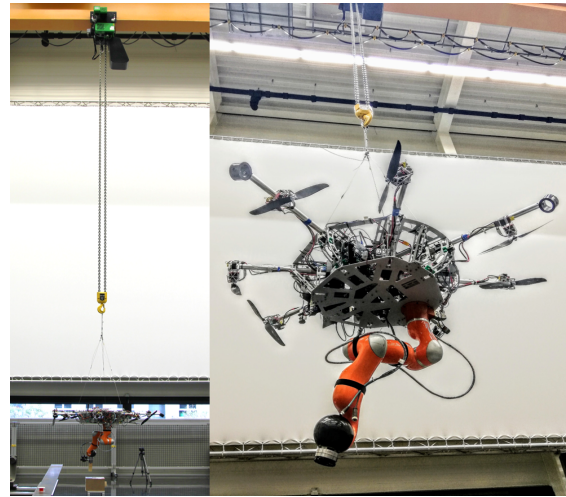
Fig. 1. Pictures of SAM.

enlarging also the spectrum of the possible applications [11]. In [12] and [13] outdoor experiments of object picking are shown using a KUKA LWR-4 directly attached to the fuselage of a helicopter. In those works, there were two main issues: the strong dynamic couplings between the aerial carrier and the manipulator, and the proximity of the large helicopter blades to the manipulation workspace.

To overcome the aforementioned problems, DLR SAM, described in detail in [14], was developed. SAM (see Fig. 1) is conceived following the emergent trend of long-reach aerial manipulators [15]–[17], i.e., separating the aerial base from the manipulation device to enhance safety and avoid the interference of rotating propellers. More in detail, SAM has a fully actuated aerial platform with eight propellers. The platform holds a 7 DoFs manipulator and is suspended through a cable below a main aerial carrier (see Fig. 1), deputed to sustaining most of the load of the system. Consequently, however, as many cable-suspended platforms, SAM suffers from the problem of oscillations since it can be seen as a pendulum [18]. However, the actuated aerial platform can be exploited to suppress the oscillations [19]. Besides damping the oscillations, the core objective is to control the end-effector of SAM to perform different tasks. In [20], a framework for bilateral teleoperation is presented that envisions a hierarchical approach in order to let the user control the aerial base attitude in the null-space of the primary task at the end-effector. That approach has been
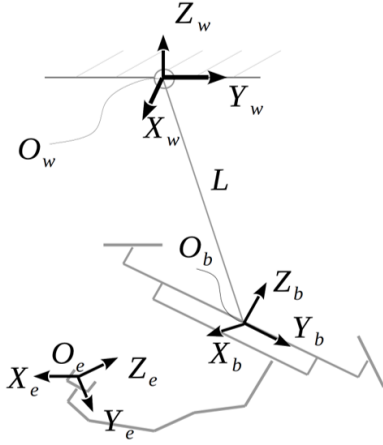
Fig. 2. Schematic representation of the system. O_w is the origin of the world-fixed frame, where a cable of length L is anchored. The other end of the cable is anchored at O_b, which is the origin of a frame attached to the aerial base. A manipulator is attached below the aerial base. A frame with origin in O_e is defined attached to the manipulator end-effector.

validated with numerical simulations using the free-flight model of SAM.

In this work, we further build upon that idea and present a strategy to achieve autonomous physical interaction tasks with SAM. Compared to [20], this paper considers the holonomic constraint imposed by the cable and applies a whole-body dynamically-decoupling control [21] to the constrained system to achieve hierarchical multi-task execution. The highest-priority task is the compliance control of the manipulator end-effector to achieve physical interaction. The second priority task is the control of the aerial base in order to damp the oscillations. An additional lower-priority task is added as the Cartesian position of the manipulator elbow, to keep the manipulation site free and damp internal redundant motions. The proposed method is validated with numerical simulations and tested on the real hardware.

II. SYSTEM MODEL

In this section, the main quantities are described together with the details about the model of the system. We suppose that the main carrier, be it a helicopter or a crane, is just deputed to bringing SAM to the location of interest and sustaining its weight. Thus, in our analysis, we consider the system schematically depicted in Fig. 2, composed of an inextensible mass-less cable anchored at a fixed point on the ceiling, a fully-actuated aerial base anchored to the cable, and a 7 DoFs manipulator attached below the platform, not necessarily at its center of mass (CoM). Note that SAM is designed so that the manipulator base is shifted w.r.t. the UAV CoM—see [14] for more details. We define an inertial frame $\{\mathscr{W}\}$ with origin O_w and axes $\{X_w, Y_w, Z_w\}$ oriented as in Fig. 2, a frame $\{\mathscr{B}\}$ fixed to the multi-rotor, with origin at its CoM, O_b, which is equivalent to the geometric center of the multi-rotor, and axes $\{X_b, Y_b, Z_b\}$. A reference frame $\{\mathscr{E}\}$ is attached to the end-effector of the arm, with origin O_e and axes $\{X_e, Y_e, Z_e\}$. We define $p_b = \begin{bmatrix} x_b & y_b & z_b \end{bmatrix}^T \in \mathbb{R}^3$

and $p_e \in \mathbb{R}^3$ as the position vectors w.r.t. $\{\mathscr{W}\}$ of $\{\mathscr{B}\}$ and $\{\mathscr{E}\}$, respectively. $(\cdot)^T$ indicates the transpose operator. We will indicate with ${}^iR_j$ the orientation of frame j w.r.t frame i, where $i, j = \{w, b, e\}$ indicate $\{\mathscr{W}\}$, $\{\mathscr{B}\}$, and $\{\mathscr{E}\}$, respectively; when i is omitted, it is intended to be $i = w$. $\zeta_e = \begin{bmatrix} \eta_e & \varepsilon_e^T \end{bmatrix}^T$ is the unit quaternion parametrizing ${}^wR_e$.

Choosing vectors $\Phi_b \in \mathbb{R}^3$ containing the three Euler angles roll, pitch, and yaw to parametrize the attitude of the aerial base, so that we have $\Phi_b = \begin{bmatrix} \phi_b & \theta_b & \psi_b \end{bmatrix}^T$, and neglecting the actuator dynamics, we define a vector $q \in \mathbb{R}^{13}$ containing the configuration variables of the overall system. Specifically, $q = \begin{bmatrix} p_b^T & \Phi_b^T & q_m^T \end{bmatrix}^T$, where $q_m \in \mathbb{R}^7$ is the vector containing the joint coordinates of the manipulator.

The cable introduces a holonomic constraint on p_b. Indicating with L the length of the cable, we have that

$$p_b^T p_b = L^2. \tag{1}$$

In our analysis, we treat the holonomic constraint at a velocity level [22]. It is worth mentioning that the constraint we are considering does not affect the attitude of the platform, but only its position. In other words, we can say that we model SAM as a double pendulum with a zero-length second link. In [19] the behavior of a double pendulum with a shorter second link is shown for the aerial base of SAM. Note also that by imposing (1) we consider that the cable is always taut, which is a common assumption in the literature [23], [24] and is particularly suited for SAM. Deriving it w.r.t time, constraint (1) can be written at a velocity level as

$$p_b^T \dot{p}_b = 0, \tag{2}$$

where the dot indicates the time derivative. Constraint (2) can be easily written in the Pfaffian form $A(q)\dot{q} = 0$ with $A(q) = \begin{bmatrix} p_b^T & 0_{1\times10} \end{bmatrix} \in \mathbb{R}^{1\times13}$, where 0 is the zero matrix with indicated dimensions. Using the Lagrangian formulation, we can write the well known dynamic equations of the constrained system as

$$M(q)\ddot{q} + C(q,\dot{q})\dot{q} + g = \tau + \tau^{ext} + A^T\lambda \tag{3}$$

$$A(q)\dot{q} = 0, \tag{4}$$

where $\lambda \in \mathbb{R}$ is a lagrangian multiplier that parametrizes the interaction forces acting along the constraint [25], $\tau = \begin{bmatrix} \tau_1 & \dots & \tau_{13} \end{bmatrix}^T$ is the control input, and $\tau^{ext} \in \mathbb{R}^{13}$ accounts for the effect of the external wrenches on the configuration space dynamics. M and C are the inertia and Coriolis matrices, respectively, and vector g contains the gravity-dependent terms. We choose a base of the null-space of $A(q)$, $S(q) \in \mathbb{R}^{13\times12}$ such that $S^T A^T = 0$. In this way, we can define the independent velocities allowed by the constraint, $\dot{\delta} \in \mathbb{R}^{12}$ such that $\dot{q} = S\dot{\delta}$ and their dynamics is

$$M_\delta(q)\ddot{\delta} + C_\delta(q,\dot{\delta})\dot{\delta} + g_\delta = \tau_\delta + \tau_\delta^{ext} \tag{5}$$

$$\dot{q} = S\dot{\delta}, \tag{6}$$

where, omitting hereinafter the dependencies for the sake of brevity, $M_\delta = S^T M S \in \mathbb{R}^{12\times12}$, $C_\delta = S^T(M\dot{S} + CS) \in \mathbb{R}^{12\times12}$, $g_\delta = S^T g \in \mathbb{R}^{12}$, $\tau_\delta = S^T \tau \in \mathbb{R}^{12}$, $\tau_\delta^{ext} = S^T \tau^{ext} \in \mathbb{R}^{12}$, and

we used $S^T A^T = 0_{12 \times 1}$ and $\ddot{q} = \dot{S}\dot{\delta} + S\ddot{\delta}$. Now, similarly to what is done in [26], we can design the control τ_δ in the constrained dynamics. Note that, in general, δ might be non-integrable and have no physical meaning; however, as we shall see, in our case it does. We choose

$$S = \begin{bmatrix} \begin{bmatrix} I_2 \\ -x_b/z_b \quad -y_b/z_b \end{bmatrix} & 0_{3 \times 10} \\ 0_{10 \times 2} & I_{10} \end{bmatrix} \quad (7)$$

where I is the identity matrix. In this way, S is always defined around our operating points, that is, when x_b, y_b are close to zero and z_b is close to $-L$. Specifically, we suppose that the system will not be working in a condition in which $x_b = \pm L$ or $y_b = \pm L$, which is a reasonable assumption always verified for SAM in practical implementations. Thus, we have $\dot{\delta} = \begin{bmatrix} \dot{x}_b & \dot{y}_b & \dot{\Phi}_b & \dot{q}_m \end{bmatrix}^T$.

We would like to stress out that a more accurate model would consider SAM as a rigid body attached to a cable whose anchoring point is not the CoM of the aerial base but a point with constant position in $\mathscr{B}$ expressed by ${}^b c_2 \in \mathbb{R}^3$. In this case, the velocity constraint would be

$$\dot{p}_b^T p_b - \dot{p}_b^T ({}^w R_b {}^b c_2) - ({}^w R_b^b c_2)^T \dot{p}_b = 0. \quad (8)$$

Constraint (1) is actually a simplification of (8) coming from imposing ${}^b c_2 = 0_{1 \times 3}$. We chose a simpler model of the constraint in this first analysis. Such a simplified model for SAM, however, would be suitable for many tethered aerial robots (see, e.g., [27], [28]). The inclusion of more accurate constraint models of SAM is left for future investigation.

III. CONTROL DESIGN

First, we consider the dynamics in (5), namely the dynamics of δ, compliant with the constraint. We can expect to control δ, but not q: in fact, z_b will be imposed by the holonomic constraint and is not arbitrarily set. We apply compliance control in the task-space using a hierarchical control approach as described in [21] to the dynamics (5).

In general, a way of exploiting robot redundancy is to simultaneously execute multiple tasks. Hierarchical control approaches are based on the prioritization of multiple tasks so that the execution of a lower priority task can be perturbed by one of a higher priority task, but not the reverse.

We define the task variables $\chi_b = \begin{bmatrix} x_b & y_b & \Phi_b^T \end{bmatrix} \in \mathbb{R}^5$, $v_b = \begin{bmatrix} \dot{x}_b & \dot{y}_b & \omega_b^T \end{bmatrix}^T$, $v_e = \begin{bmatrix} \dot{p}_e^T & \omega_e^T \end{bmatrix}^T$, with ω_b, ω_e angular velocities of $\mathscr{B}$ and $\mathscr{E}$, respectively, and x_{elbow} the coordinate of the Cartesian position of the manipulator elbow, expressed in $\{\mathscr{W}\}$. Control of the elbow has been considered for ground mobile manipulators [29] to maintain a more compact configuration of the arm. It could be also useful to obtain arm configurations that keep the manipulation site as free as possible, and to help damping internal motions of the arm.

Let us define the task jacobians J_i, where a higher value of i indicates a higher priority task. Particularly, $J_1 \in \mathbb{R}^{6 \times 12}$ is such that $v_e = J_1 \dot{\delta}$, $J_2 \in \mathbb{R}^{5 \times 12}$ is such that $v_b = J_2 \dot{\delta}$ and $J_3 \in \mathbb{R}^{1 \times 12}$ such that $\dot{x}_{elbow} = J_3 \dot{\delta}$. We stack the ordered task jacobians: $J_i^{\text{aug}} = \begin{bmatrix} J_1^T & \dots & J_i^T \end{bmatrix}^T$ and we define the task hierarchy: $\bar{J} = \begin{bmatrix} J_1^T & \bar{J}_2^T & \bar{J}_3^T \end{bmatrix}^T \in \mathbb{R}^{12 \times 12}$, where, for

$i = 2, \dots, 3$, we have $\bar{J}_i = J_i N_i^T$ with $N_i = I - J_{i-1}^{\text{aug}} J_{i-1}^{\text{aug},M_\delta+,T}$ and $A^{M_\delta+} = M_\delta^{-1} A^T (A M_\delta^{-1} A^T)^{-1}$ a dynamically consistent pseudoinversion [30]. $\bar{J}$ can be interpreted as the following coordinate transformation:

$$\begin{bmatrix} v_1 \\ v_2 \\ v_3 \end{bmatrix} = \bar{J}\dot{\delta}, \quad (9)$$

where $v_1 = v_e$. Note that N_i is used to project lower priority tasks into the null space of the higher priority ones. Therefore, e.g., v_2 lives in the null-space of J_1.

Using the coordinate transformation (9), the dynamics (5) can be rewritten as

$$\Lambda \dot{v} + \Gamma v = \bar{J}^{-T} (\tau_\delta + \tau_\delta^{ext} + g_\delta), \quad (10)$$

where $\Lambda = \bar{J}^{-T} M_\delta \bar{J}^{-1}$, and $\Gamma = \bar{J}^{-T} (C_\delta - M_\delta \dot{\bar{J}}) \bar{J}^{-1}$. It is worthwhile to mention that the use of dynamically consistent pseudoinverse leads to decoupling of v_i in the acceleration level [30], meaning that the inertia matrix Λ is block diagonal. Now, we can write the control law as:

$$\tau_\delta = \tau_\Gamma + g_\delta + J_1^T f_{1,\text{ctrl}} + \sum_{i=2}^{3} N_i J_i^T f_{i,\text{ctrl}}, \quad (11)$$

where $\tau_\Gamma = \sum_{i_1}^{3} (\bar{J}_i^T (\sum_{j=1}^{i-1} \Gamma_{i,j} v_j) + \sum_{j=i+1}^{3} \Gamma_{i,j} v_j)$ with $i, j = 1, \dots, 3$ indicating the corresponding task, and $\Gamma_{i,j}$ referring to the block of matrix Γ obtained extracting rows corresponding to task i and columns to task j. Basically, τ_Γ cancels out the outer diagonal terms of the Coriolis and centrifugal components in (10).

To summarize, due to the dynamically consistent projection, the control input $f_{2,\text{ctrl}}$ does not influence the variable $v_1 = v_e$, and $f_{3,\text{ctrl}}$ does not influence the variables v_1 and v_2. Therefore, we use $f_{1,\text{ctrl}}$ for the compliance control of the manipulator:

$$f_{1,\text{ctrl}} = \begin{bmatrix} -K_{1,p}(p_e - p_e^d) \\ -2^e R_e^d E(\eta^d, \varepsilon^d)^T R_e^{dT} K_{1,o}^w R_e^d \varepsilon^d \end{bmatrix} - D_1 v_e. \quad (12)$$

Lower priority control inputs are defined by

$$f_{2,\text{ctrl}} = -K_2(\chi_b - \chi_b^d) - D_2 v_b, \quad (13)$$

$$f_{3,\text{ctrl}} = -K_3(x_{elbow} - x_{elbow}^d) - D_3 \dot{x}_{elbow}. \quad (14)$$

Here, $(\cdot)^d$ indicates the corresponding desired quantity, and $K_{1,p}, K_{1,o}, D_1, K_2, D_2, K_3, D_3$ are constant positive-definite and symmetric gain matrices of appropriate dimensions, and $E(\eta^d, \varepsilon^d) = \eta^d I_3 - \hat{\varepsilon}^d$ [31], where the hat indicates the skew operator. We remark that the compliance controller (11) does not require the feedback of any external wrench.

To implement controller (11) on the actual system, we need to define $\tau \in \mathbb{R}^{13}$, the actual control input of our system. To do so, [32] proposes the following transformation:

$$\tau = \begin{bmatrix} ((S^T M S)^{-1} S^T M)^T & A^T \end{bmatrix} \begin{bmatrix} \tau_\delta \\ \tau_\xi \end{bmatrix}, \quad (15)$$

where τ_ξ is the component of the control along the constraints. In our case, τ_ξ has been simply set to zero because we do not want to apply any control action along the constraint.
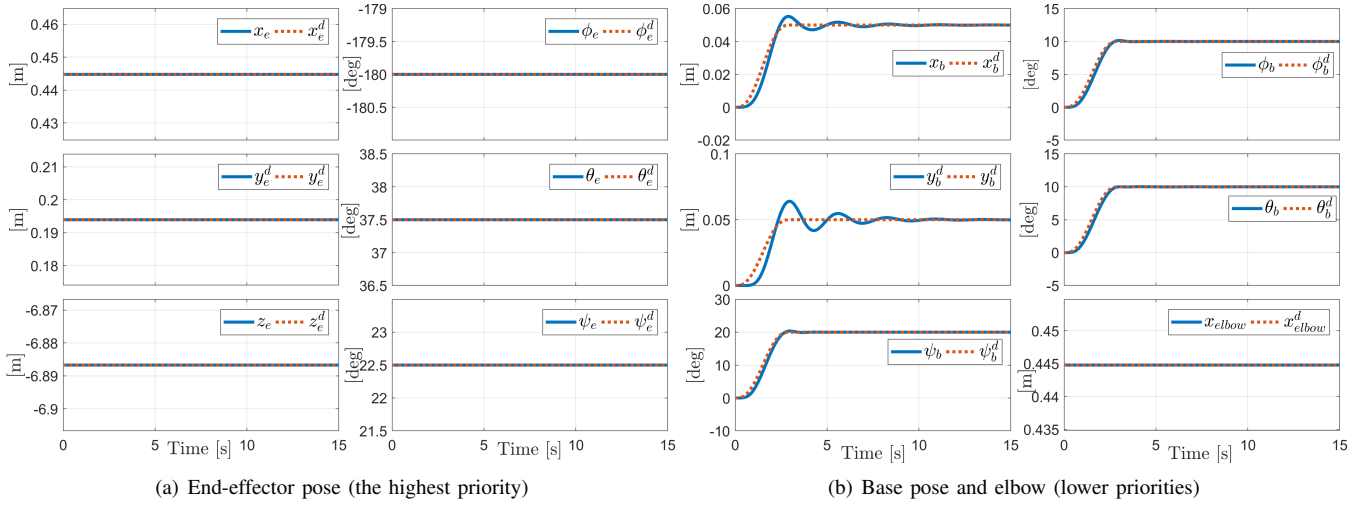
(a) End-effector pose (the highest priority)   (b) Base pose and elbow (lower priorities)

Fig. 3.   Simulated scenario1. The first priority task on the end-effector is not perturbed during lower priority tasks execution.

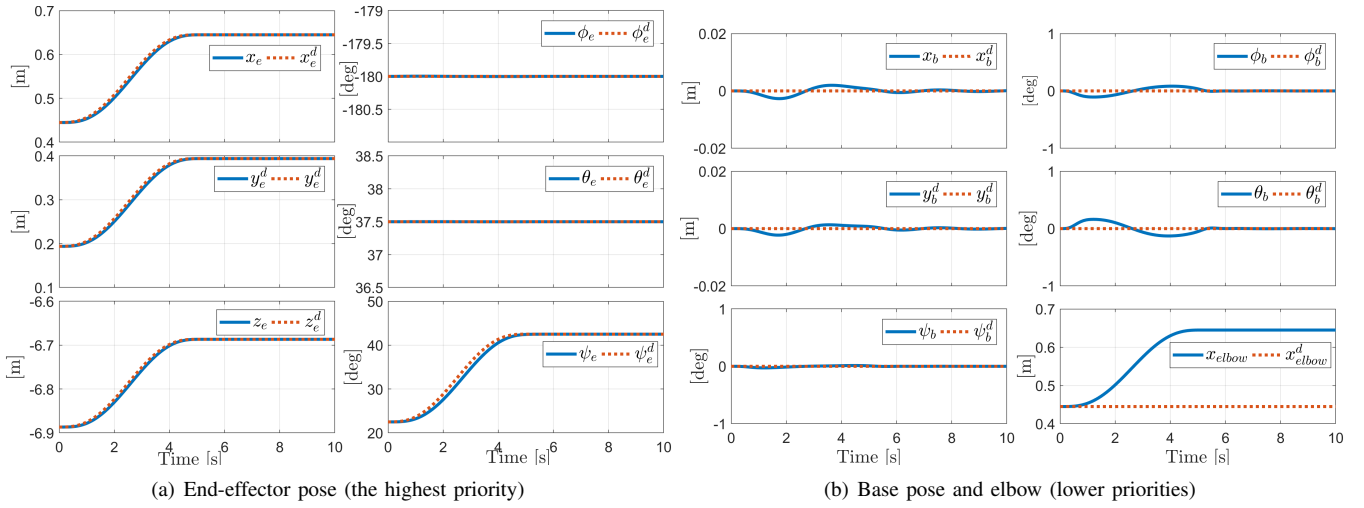(a) End-effector pose (the highest priority)   (b) Base pose and elbow (lower priorities)

Fig. 4.   Simulated scenario2. Lower priority tasks are perturbed during highest priority task execution.

(a)   (b)
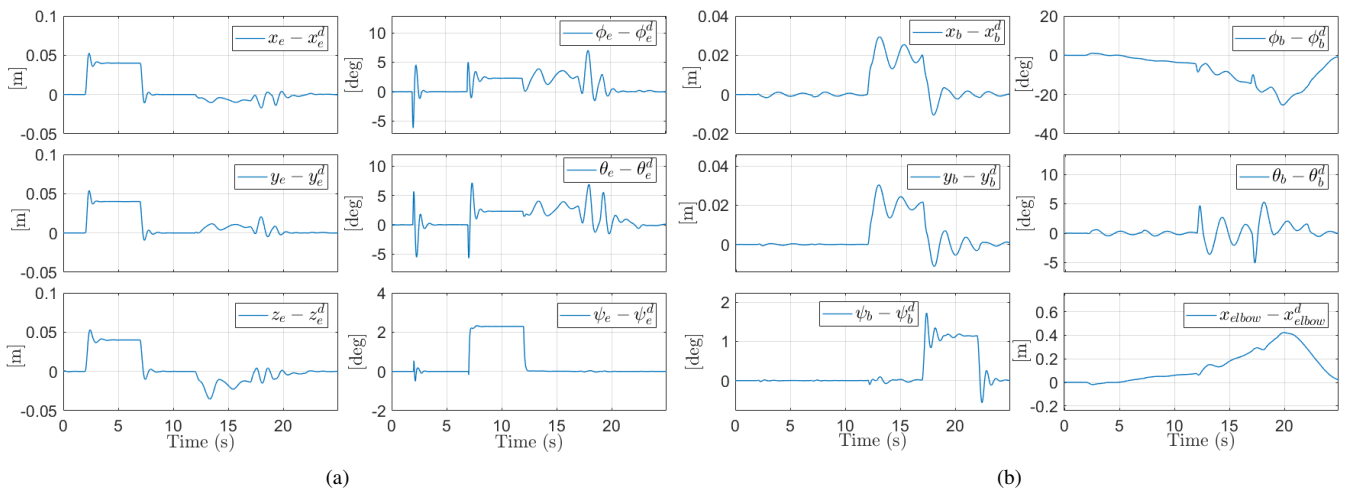
Fig. 5.   Simulated scenario3. Constant reference equal to their initial values are imposed on χ_e, χ_b and x_{elbow} while external wrenches are applied to the end-effector and to the aerial base CoM.
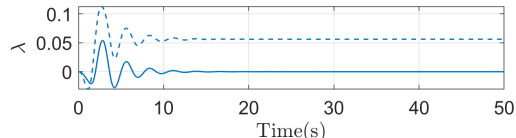
Fig. 6. Evolution of parameter λ in simulated scenario1 not considering gravity, applying (11) and an analogous control but based on the unconstrained (free-flight) dynamic model—dashed line. In the latter case, a constant reference altitude is commanded to the aerial base, which is unfeasible due to the cable. After the reaction force enforces the constrained motion, at steady state $\lambda \neq 0$, since the robot tries to oppose to the constraint and bring itself to the unfeasible configuration, also wasting control effort.

From one side, the advantage of using a constraint-aware control law instead of treating SAM as a free-flight platform is that this avoids generating unnecessary stress in the mechanical constraint and thus external forces on the robot. From the other side, we do not spend a portion of the control energy in a direction in which it does not have any useful effect, optimizing the power consumption of the multi-rotor—see also Fig. 6.

IV. SIMULATIONS

Three different scenarios were simulated in Matlab-Simulink using the dynamics computation algorithm proposed in [33]. In scenario1 and scenario2, reference poses are assigned to the end-effector and to the aerial base to assess if the hierarchical control structure works as expected. In scenario3 external forces and torques are applied to the system to assess the compliant behavior of the controller.

The cable length is $L = 6$m, the mass of the aerial base $m_b = 30$kg, and its inertia $I_b = \mathrm{diag}(4.2, 4.2, 8.4)$kgm^2. All parameters have been chosen as close as possible to the real system. The controller gains are $K_{1,p} = K_{1,o} = K_2 = K_3 = 500$N/m, and $D_1 = D_2 = D_3 = 200$Ns/m. Even though (12) uses quaternions for the parameterization of the attitude of the end effector, Euler angles are used in the figures to report results in a more intuitive form. We define $\chi_e = \begin{bmatrix} p_e^{\mathrm{T}} & \Phi_e^{\mathrm{T}} \end{bmatrix}^T \in \mathbb{R}^6$, where $\Phi_e = \begin{bmatrix} \phi_e & \theta_e & \psi_e \end{bmatrix}^T$ is the vector containing roll, pitch and yaw angles of the end effector.

Fig. 3 shows the results of the simulated scenario1. The desired pose of the end-effector is equal to its initial pose. $x_b^d = x_b + 0.05$m, $y_b^d = y_b + 0.05$m, $\Phi_b^d = \Phi_b + \begin{bmatrix} 10 & 10 & 10 \end{bmatrix}^T$ deg, and x_{elbow}^d is set equal to its initial value. Ppolynomial trajectories of the 5$^{\mathrm{th}}$-order between the initial and desired pose are given as references. Fig. 4 reports the results of the simulated scenario2. In this case, the aerial base and the elbow are controlled to their constant initial poses, while the end-effector moves to follow a reference. Particularly, $p_e^d = p_e + \begin{bmatrix} 0.2 & 0.2 & 0.2 \end{bmatrix}^T$ m and $\Phi_b^d = \Phi_b + \begin{bmatrix} 0 & 0 & 20 \end{bmatrix}^T$ deg. The results of these simulations validate the proposed hierarchical control structure since in scenario1 the end-effector (first priority task) keeps its position, not perturbed by lower priority tasks while, in contrast, in scenario2 the lower priority tasks are perturbed by the end-effector motion.

Fig. 5 shows the results of simulated scenario3. Both χ_e and χ_b are regulated to their initial values. Between time $t = 2$s and time $t = 7$s an external force acts on the end effector, with an intensity of 20N in each direction; between $t = 7$s and $t = 12$s an external torque of 20Nm in each direction acts on the end-effector. Between $t = 12$s and $t = 17$s an external force with an intensity of 10N in each direction acts on the CoM of the aerial base, while an external torque of 10Nm in each direction acts on it between $t = 17$s and $t = 22$s. The system shows compliant behavior under physical interactions. We recall that no feedback of external wrenches is used for the control.

V. EXPERIMENTS

The proposed controller has been implemented on SAM. One difference with respect to the numerical validation is that we had to slightly modify the control for the secondary task. In the simulation, we used (13) which is basically a PD controller that requires the full state of the system. However, in the real system, we cannot measure the full state using a single onboard IMU.[1] To overcome this problem, we calculate linear velocities in (13) by using ω_b^{lp}, where ω_b^{lp} is the low-pass filtered value of the angular velocity measured by IMU. Conceptually speaking, ω_b^{lp} filters out the oscillations of the second pendulum joint of SAM so that only the oscillations of the first pendulum joint remain. This statement is true because of the nature of the double pendulum with the first cable longer than the second one. For further details, please refer to [19]. We remark that, based on our experience, oscillation damping plus yaw control is sufficient for our purposes.

Two experiments in an indoor environment (see Fig. 1) were carried out. With the first experiment, we wanted to assess the compliant behavior during strong physical interaction. The manipulator end-effector was punched by a wooden stick with considerable force in order to disturb it. χ_e^d was set constant and equal to the initial value of χ_e. The oscillations were damped while χ_e returned to its controlled pose after the contact. A photo sequence of this experiment is shown in Fig. 7(a), while corresponding plots are reported in Fig. 8. Oscillations of small intensity, actually, do persist. This is due to the non-perfect oscillation-damping control, which we intend to improve through a refinement of the system model.

The goal of the second experiment was to perform a task in which the manipulator end-effector is in contact with the environment. For this purpose, a wooden rigid tool was attached to the end-effector. The manipulator has been given a reference trajectory in order to push against an open drawer and close it. The secondary task that damps the oscillations of the aerial base tended to keep it steady during the execution. A photo sequence of this experiment is shown in Fig. 7(b), while corresponding plots are reported in Fig. 9. Please see also the video of the experiments, attached to this work.

---

[1] Since we target manipulation in complex environments, we try not to use vision and/or GPS-based positioning for the attitude control.
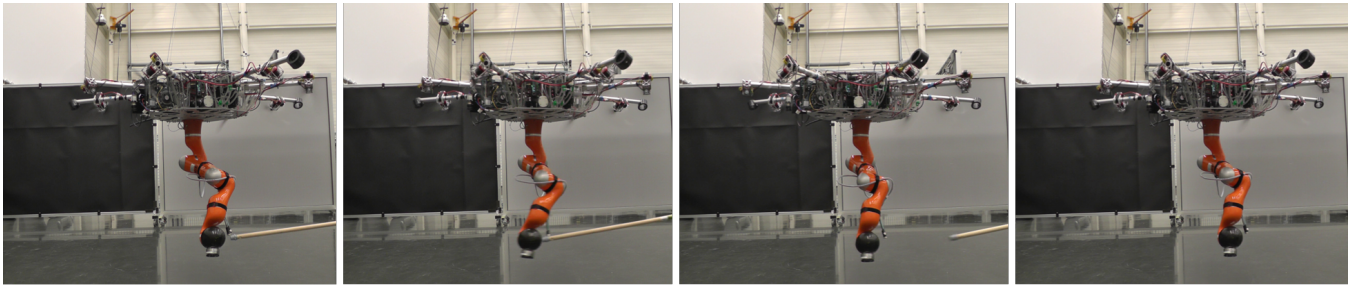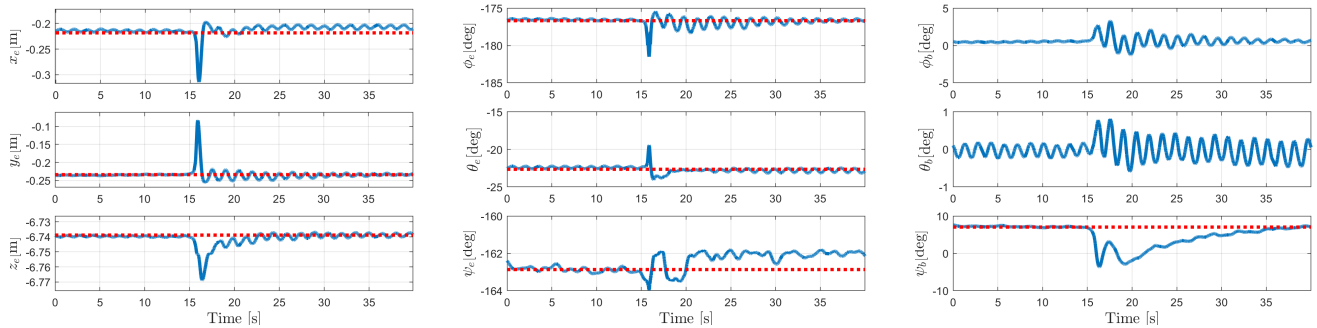
(a) SAM end-effector is perturbed by an external force to assess the stability under strong physical interaction.
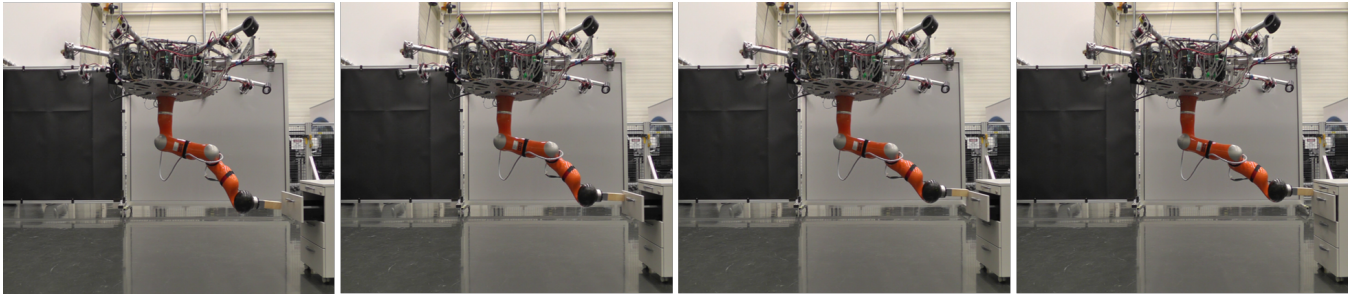
(b) SAM, equipped with a rigid wooden end-effector, closes a drawer while the perturbations on the slung aerial base are damped.

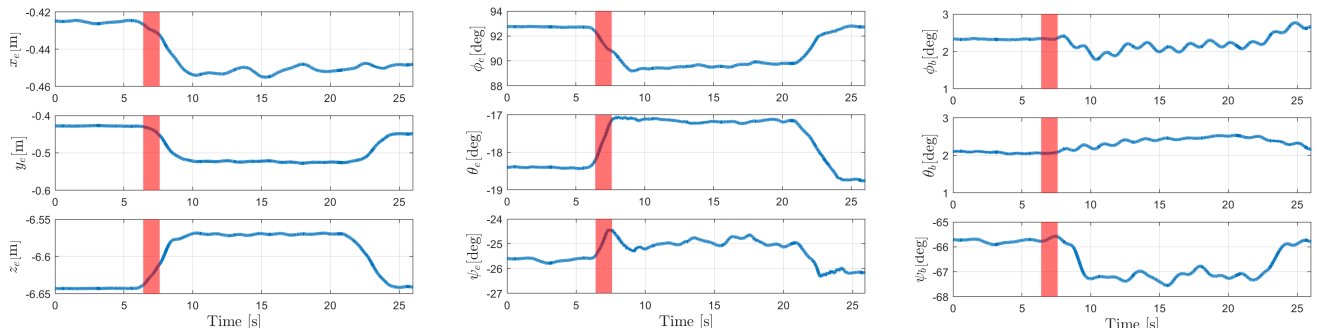Fig. 7. Photo-sequences of two experiments on SAM.

(a) End-effector position.

(b) End-effector attitude

(c) aerial base attitude

Fig. 8. Results of the experiment reported in Fig. 7(a). It is clear from the graphs the moment when the end-effector is pushed by the wooden stick. The compliance controller keeps the robot stable during strong physical interaction.

(a) End-effector position.

(b) End-effector attitude

(c) aerial base attitude

Fig. 9. Results of the experiment reported in Fig. 7(b). The manipulator end-effector follows a trajectory to push the drawer while the aerial base damps the induced oscillations. The red vertical stripes in the plots indicate when the robot starts making contact with the environment.

VI. CONCLUSIONS

We presented a control method for a cable-suspended aerial manipulator, tested with numerical simulations and experiments on the DLR SAM. The constrained system was modeled, and hierarchical compliance control in the operational space was applied. Control of the manipulator

end-effector pose was the highest priority task, while secondary task damps oscillations. A third priority task was implemented on the position of the manipulator elbow.

Future work will focus on the inclusion of a more complex model of the constraint in the system. The feedback of the external wrenches acting on the end-effector could be exploited to perform interaction tasks that require higher accuracy in this respect. The improvements will be tested in the complex outdoor environment.

REFERENCES

[1] H. B. Khamseh, F. Janabi-Sharifi, and A. Abdessameud, "Aerial manipulation—a literature survey," *Robotics and Autonomous Systems*, vol. 107, pp. 221–235, 2018.

[2] A. Ollero, G. Heredia, A. Franchi, G. Antonelli, K. Kondak, A. Sanfeliu, A. Viguria, J. R. Martinez-de Dios, F. Pierri, J. Cortes, A. Santamaria-Navarro, M. A. Trujillo Soto, R. Balachandran, J. Andrade-Cetto, and A. Rodriguez, "The aeroarms project: Aerial robots with advanced manipulation capabilities for inspection and maintenance," *IEEE Robotics and Automation Magazine (RA-M)*, vol. 25, no. 4, pp. 12–23, Dec 2018.

[3] M. Ryll, G. Muscio, F. Pierri, E. Cataldi, G. Antonelli, F. Caccavale, and A. Franchi, "6d physical interaction with a fully actuated aerial robot," in *IEEE International Conference on Robotics and Automation (ICRA)*, 2017, pp. 5190–5195.

[4] C. Gabellieri, M. Tognon, D. Sanalitro, L. Pallottino, and A. Franchi, "A study on force-based collaboration in swarms," *Swarm Intelligence*, vol. 14, no. 1, pp. 57–82, 2020.

[5] D. Mellinger, M. Shomin, N. Michael, and V. Kumar, "Cooperative grasping and transport using multiple quadrotors," in *Distributed autonomous robotic systems*. Springer, 2013, pp. 545–558.

[6] M. J. Kim, K. Kondak, and C. Ott, "A stabilizing controller for regulation of uav with manipulator," *IEEE RA-L*, vol. 3, no. 3, pp. 1719–1726, 2018.

[7] F. Ruggiero, V. Lippiello, and A. Ollero, "Aerial manipulation: A literature review," *IEEE Robotics and Automation Letters (RA-L)*, vol. 3, no. 3, pp. 1957–1964, 2018.

[8] S. Kim, S. Choi, and H. J. Kim, "Aerial manipulation using a quadrotor with a two dof robotic arm," in *IEEE/RSJ International Conference on Intelligent Robots and Systems (IROS)*, 2013, pp. 4990–4995.

[9] S. Kim, H. Seo, S. Choi, and H. J. Kim, "Vision-guided aerial manipulation using a multirotor with a robotic arm," *IEEE/ASME Transactions On Mechatronics*, vol. 21, no. 4, pp. 1912–1923, 2016.

[10] S. Kim, H. Seo, and H. J. Kim, "Operating an unknown drawer using an aerial manipulator," in *IEEE International Conference on Robotics and Automation (ICRA)*, 2015, pp. 5503–5508.

[11] M. J. Kim, R. Balachandran, M. De Stefano, K. Kondak, and C. Ott, "Passive compliance control of aerial manipulators," in *IEEE/RSJ International Conference on Intelligent Robots and Systems (IROS)*, 2018, pp. 4177–4184.

[12] F. Huber, K. Kondak, K. Krieger, D. Sommer, M. Schwarzbach, M. Laiacker, I. Kossyk, S. Parusel, S. Haddadin, and A. Albu-Schäffer, "First analysis and experiments in aerial manipulation using fully actuated redundant robot arm," in *IEEE/RSJ International Conference on Intelligent Robots and Systems (IROS)*, 2013, pp. 3452–3457.

[13] K. Kondak, F. Huber, M. Schwarzbach, M. Laiacker, D. Sommer, M. Bejar, and A. Ollero, "Aerial manipulation robot composed of an autonomous helicopter and a 7 degrees of freedom industrial manipulator," in *IEEE International Conference on Robotics and Automation (ICRA)*, 2014, pp. 2107–2112.

[14] Y. S. Sarkisov, M. J. Kim, D. Bicego, D. Tsetserukou, C. Ott, A. Franchi, and K. Kondak, "Development of sam: cable-suspended aerial manipulator," in *IEEE International Conference on Robotics and Automation (ICRA)*, May 2019, pp. 5323–5329.

[15] A. Caballero, A. Suarez, F. Real, V. M. Vega, M. Bejar, A. Rodriguez-Castaño, and A. Ollero, "First experimental results on motion planning for transportation in aerial long-reach manipulators with two arms," in *IEEE/RSJ International Conference on Intelligent Robots and Systems (IROS)*, 2018, pp. 8471–8477.

[16] A. Suárez, P. Sanchez-Cuevas, M. Fernandez, M. Perez, G. Heredia, and A. Ollero, "Lightweight and compliant long reach aerial manipulator for inspection operations," in *IEEE/RSJ International Conference on Intelligent Robots and Systems (IROS)*, 2018, pp. 6746–6752.

[17] R. Miyazaki, R. Jiang, H. Paul, Y. Huang, and K. Shimonomura, "Long-reach aerial manipulation employing wire-suspended hand with swing-suppression device," *IEEE Robotics and Automation Letters (RA-L)*, vol. 4, no. 3, pp. 3045–3052, 2019.

[18] I. Palunko, P. Cruz, and R. Fierro, "Agile load transportation: Safe and efficient load manipulation with aerial robots," *IEEE Robotics and Automation Magazine (RA-M)*, vol. 19, no. 3, pp. 69–79, 2012.

[19] Y. Sarkisov, M. J. Kim, A. Coelho, D. Tsetserukou, C. Ott, and K. Kondak, "Optimal oscillation damping control of cable-suspended aerial manipulator with a single imu sensor," in *2020 IEEE International Conference on Robotics and Automation (ICRA)*, 2020, pp. 5349–5355.

[20] A. Coelho, H. Singh, K. Kondak, and C. Ott, "Whole-body bilateral teleoperation of a redundant aerial manipulator," in *2020 IEEE International Conference on Robotics and Automation (ICRA)*, 2020, pp. 9150–9156.

[21] A. Dietrich and C. Ott, "Hierarchical impedance-based tracking control of kinematically redundant robots," *IEEE Transactions on Robotics*, 2019.

[22] Xiaoping Yun and N. Sarkar, "Unified formulation of robotic systems with holonomic and nonholonomic constraints," *IEEE Transactions on Robotics and Automation*, vol. 14, no. 4, pp. 640–650, Aug 1998.

[23] C. Masone, H. H. Bülthoff, and P. Stegagno, "Cooperative transportation of a payload using quadrotors: A reconfigurable cable-driven parallel robot," in *2016 IEEE/RSJ IROS*. IEEE, 2016, pp. 1623–1630.

[24] M. Tognon, C. Gabellieri, L. Pallottino, and A. Franchi, "Aerial co-manipulation with cables: The role of internal force for equilibria, stability, and passivity," *IEEE Robotics and Automation Letters*, vol. 3, no. 3, pp. 2577–2583, 2018.

[25] B. Siciliano, L. Sciavicco, L. Villani, and G. Oriolo, *Robotics: modelling, planning and control*. Springer-Verlag, 2009.

[26] G. Zambella, G. Lentini, M. Garabini, G. Grioli, M. G. Catalano, A. Palleschi, L. Pallottino, A. Bicchi, A. Settimi, and D. Caporale, "Dynamic whole-body control of unstable wheeled humanoid robots," *IEEE Robotics and Automation Letters*, vol. 4, no. 4, pp. 3489–3496, 2019.

[27] M. M. Nicotra, R. Naldi, and E. Garone, "Taut cable control of a tethered uav," *IFAC Proceedings Volumes*, vol. 47, no. 3, pp. 3190–3195, 2014.

[28] M. Tognon, S. S. Dash, and A. Franchi, "Observer-based control of position and tension for an aerial robot tethered to a moving platform," *IEEE Robotics and Automation Letters (RA-L)*, vol. 1, no. 2, pp. 732–737, 2016.

[29] M. Iskandar, G. Quere, A. Hagengruber, A. Dietrich, and J. Vogel, "Employing whole-body control in assistive robotics," in *IEEE/RSJ International Conference on Intelligent Robots and Systems (IROS)*, 2019, pp. 5643–5650.

[30] A. Dietrich, C. Ott, and A. Albu-Schäffer, "An overview of null space projections for redundant, torque-controlled robots," *The International Journal of Robotics Research (IJRR)*, vol. 34, no. 11, pp. 1385–1400, 2015.

[31] S. Zhang and E. D. Fasse, "Spatial compliance modeling using a quaternion-based potential function method," *Multibody System Dynamics*, vol. 4, no. 1, pp. 75–101, 2000.

[32] D. Lee, "Passive decomposition and control of nonholonomic mechanical systems," *IEEE Transactions on Robotics (T-RO)*, vol. 26, no. 6, pp. 978–992, 2010.

[33] G. Garofalo, C. Ott, and A. Albu-Schäffer, "On the closed form computation of the dynamic matrices and their differentiations," in *IEEE/RSJ International Conference on Intelligent Robots and Systems (IROS)*, 2013, pp. 2364–2359.